A toxin-antitoxin system provides phage defense via DNA damage and repair

Huan Pu[1], Yuxin Chen[1], Xinjun Zhao[2], Lunzhi Dai [2], Aiping Tong [1], Dongmei Tang[3] ✉, Qiang Chen [1] ✉ & Yamei Yu [1] ✉

Widespread in bacteria and archaea, toxin-antitoxin (TA) systems have been recently demonstrated to function in phage defense. Here we characterize the anti-phage function of a type IV TA system, ShosTA. Using structural and biochemical approaches, we show that ShosT couples phosphoribosyl-transferase and pyrophosphatase activities to disrupt purine metabolism, resulting in DNA duplication, cell filamentation and ultimate cell death. ShosA binds DNA and likely recruits other proteins to facilitate DNA homologous recombination to antagonize ShosT's toxicity. We identify Gp0.7 of T7 phage as a trigger for ShosTA system via shutting off the protein synthesis, and the C-terminus-mediated intrinsic instability of ShosA releases the toxicity of the existing ShosT proteins. Collectively, our results provide a novel toxin-antitoxin mechanism for anti-phage immunity and shed light on the triggering of this TA system.

Toxin-antitoxin (TA) systems are broadly distributed throughout bacteria and archaea, which usually contain a toxin and a cognate antitoxin[1]. The known TA systems could be classified into eight major types, according to the nature and mode of action of antitoxins[2]. Despite the seemingly high cost for the host cell to maintain the TA systems in an 'off' state, the prevalence of TA systems implies that they play an essential role for bacterial survival. Although the plasmid-encoded TA systems serve to maintain plasmids in bacterial populations, known as "plasmid addiction"[3], the biological functions of chromosomally-encoded TA systems have remained elusive and controversial[4–6]. Recently, accumulated evidence suggested that TA systems are involved in phage defense, and the mechanisms of these anti-phage TA systems have become a particularly active research topic[7,8].

Due to the inherent toxicity, TA systems are thought to mediate abortive infection (Abi), wherein the infected host cell commits altruistic suicide before the phage completes its replication cycle and prevents the phage epidemic. Some anti-phage TA systems have been characterized, revealing diverse mechanisms that toxins use against phage infection. The type II system RnlAB and type III system ToxIN are both featured by an RNase toxin activated by T4-induced shutoff of host transcription[9]. The Type II TA system CapRel is activated by newly synthesized phage major capsid protein, releasing tRNA-targeted toxicity[10]. DarTG provides defense against phage through DNA ADP-ribosyltransferase activity[11]. Retron-Sen2 and CmdTAC are both tripartite TA systems, with toxic N-glycosidase and ADP-ribosyltransferase effector proteins, respectively[12,13].

Here, we structurally and biochemically characterize a recently identified anti-phage TA system, ShosTA[14–16]. This defense system comprises two components, the toxin ShosT and the cognate antitoxin ShosA. We reveal that ShosT couples phosphoribosyltransferase (PRTase) and pyrophosphatase (PPase) activities to disrupt purine metabolism, resulting in DNA duplication, cell filamentation and ultimate cell death. ShosA binds DNA and likely recruits other proteins to facilitate DNA repair to antagonize ShosT's toxicity. We demonstrate that Gp0.7 of T7 phage inhibits host transcription and shuts off the synthesis of ShosT and ShosA, and the intrinsic instability of ShosA breaks the toxin-antitoxin balance. The existing pool of ShosT then results in cell death which provides phage resistance via Abi mechanism. Our study represents a new toxin-antitoxin mechanism of action

[1]Department of Biotherapy, Cancer Center and State Key Laboratory of Biotherapy, West China Hospital, Sichuan University, Chengdu 610041, China. [2]National Clinical Research Center for Geriatrics, State Key Laboratory of Biotherapy, West China Hospital, Sichuan University, Chengdu 610041, China. [3]Department of Urology, State Key Laboratory of Biotherapy, West China Hospital, Sichuan University, Chengdu 610041, China. ✉e-mail: dongmeitang@scu.edu.cn; qiang_chen@scu.edu.cn; yamei_yu@scu.edu.cn

for anti-phage defense and provides insights into the intrinsic instability of the antitoxin and the triggering of the toxin.

Results

ShosTA system provided defense against phages

The ShosTA system has been previously shown to function in phage defence[15,16]. To further evaluate the phage defense provided by ShosTA, we synthesized the *shosA* and *shosT* genes of *E. coli* APEC O1 (Fig. 1a), under the control of its native promoter, into *E. coli* BL21(DE3) which naturally lacks these genes. We challenged the ShosTA-containing strain with a set of phages, including all three morphological families of the Caudovirales (P1, T2 and T4 from the Myoviridae, T5 from the Siphoviridae, and T7 from the Podoviridae) (Fig. 1b). We found that this ShosTA system protected *E. coli* against T7, reducing plating efficiency by 6 orders of magnitude (Fig. 1b).

TA systems usually mediate bacterial immunity via abortive infection (Abi) due to the inherent toxicity of the toxin. To test whether the ShosTA system triggers Abi, we infected cells harboring either the empty vector or the native ShosTA system with T7 phage at varying MOIs (multiplicity of infection). While the cultured ShosTA-containing bacteria continued to grow at low MOIs, a high MOI of 2 abolished the growth of the bacterial population, representing a key characteristic of Abi mechanisms (Fig. 1c). Since the infected cell needs to commit suicide before the completion of the phage replication cycle to protect the bacterial colony, the typical Abi usually shows an earlier culture collapse for the system-containing cells compared to those lacking the system. However, we have not observed the earlier culture collapse at the high MOI (Fig. 1c).

To confirm that ShosTA is a functional toxin-antitoxin system, we expressed ShosT alone or co-expressed ShosT with ShosA in *E. coli* BL21-AI and examined the colony forming units (CFU). With increasing arabinose inducing concentration, a marked decrease of CFU was observed for ShosT alone, while the co-expression of ShosT and ShosA showed no significant difference compared to the noninduced sample (Fig. 1d). The colony forming assay confirmed that ShosT and ShosA are toxin and antitoxin, respectively.

Crystal structure and enzymatic activities of ShosT

Due to its toxicity, ShosT is hard to express alone in *E. coli*. We co-expressed ShosT with ShosA and purified it to homogeneity. ShosT was expressed with an N-terminal His6 tag while ShosA was expressed in its native form. Only ShosT was purified from Ni^{2+} affinity column, implying there was no direct interaction between ShosT and ShosA.

To further understand the molecular basis of the toxin ShosT, we determined the crystal structure of ShosT at 1.7-Å resolution. ShosT adopted a two-domain architecture consisting of an N-terminal hydrolase domain (residues 1–164) and a C-terminal phosphoribosyltransferase (PRTase) domain (residues 165–424) (Fig. 2a).

The N-terminal hydrolase domain of ShosT represented a Rossmann-fold core, in which a central five-stranded parallel β-sheet (β5-β2-β1-β6-β7) was packed with five surrounding α helixes and an additional two-stranded antiparallel β-sheet (β3-β4) (Fig. 2b). Structural comparison showed that ShosT's N-terminal hydrolase domain shared a clear homology with the type III soluble inorganic pyrophosphatases (PPase)[17] (Fig. 2c). Since the structural analysis indicated an inorganic pyrophosphatase activity for the N-terminal hydrolase domain of ShosT, we evaluated the hydrolysis of inorganic pyrophosphate (PPi) of ShosT by monitoring the PPi consumption. ShosT showed a clear pyrophosphatase activity in vitro in a Mg^{2+}-independent manner (Fig. 2d).

Then we attempted to co-crystallize ShosT with PPi. However, in the crystal structure, we only found the hydrolysis product, orthophosphate, in the active site of ShosT's hydrolase domain (Fig. 2e).
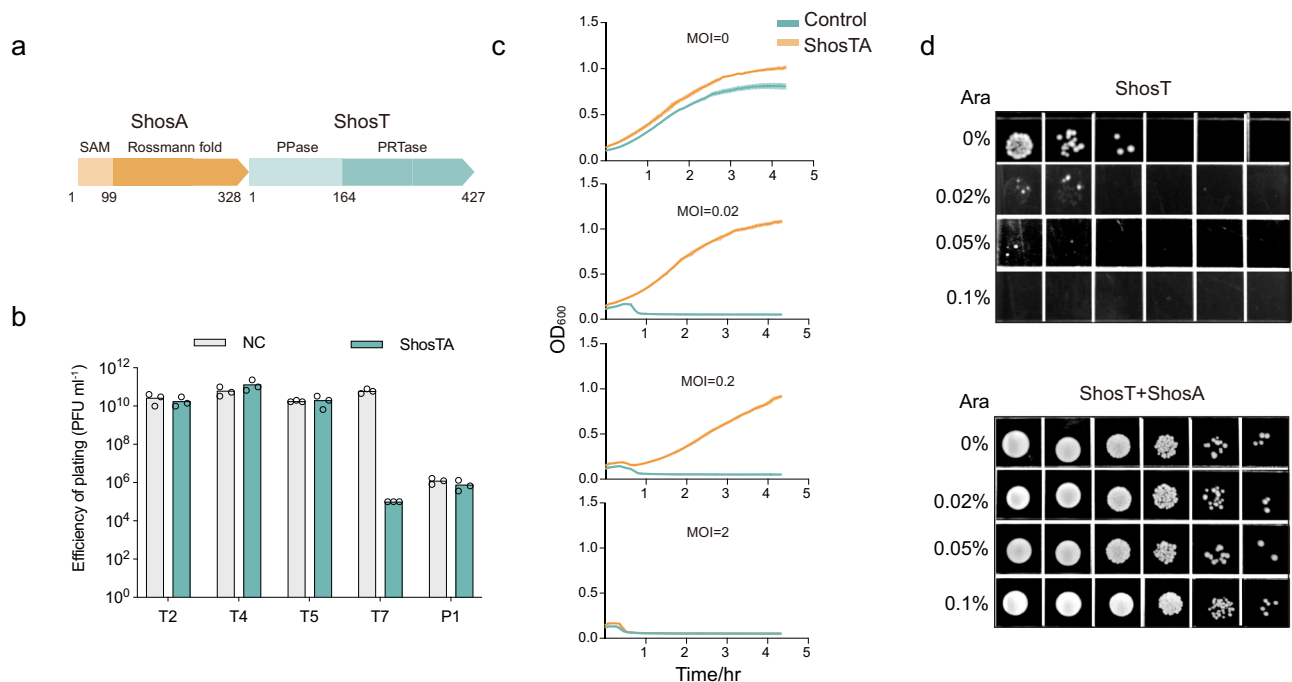

Fig. 1 | ShosTA system provides anti-phage defense via toxin-antitoxin mechanism. a Schematic diagram of ShosTA system. The boundaries for each domain are labeled. **b** Plating efficiency of various phages infecting the *E. coli* BL21(DE3) strain containing empty vector or ShosTA system. Data represent plaque-forming units (PFUs) per milliliter of each phage infection. Bar graphs show the average of three replicates with individual data points overlaid. **c** Phage infection in liquid cultures of the *E. coli* BL21(DE3) strain containing ShosTA system. The strain containing empty vector is used as the control. Cells are infected at various MOI values. For each MOI, results of three experiments are presented as the average of three replicates with shaded areas indicating SD. Source data are provided as a Source Data file. **d** Representative plating assay showing ShosA rescue of ShosT toxicity. Plasmids harboring ShosT or ShosTA under arabinose-inducible promoters, respectively, are transformed into *E. coli* BL21-AI. The arabinose concentrations used for inducing are indicated.
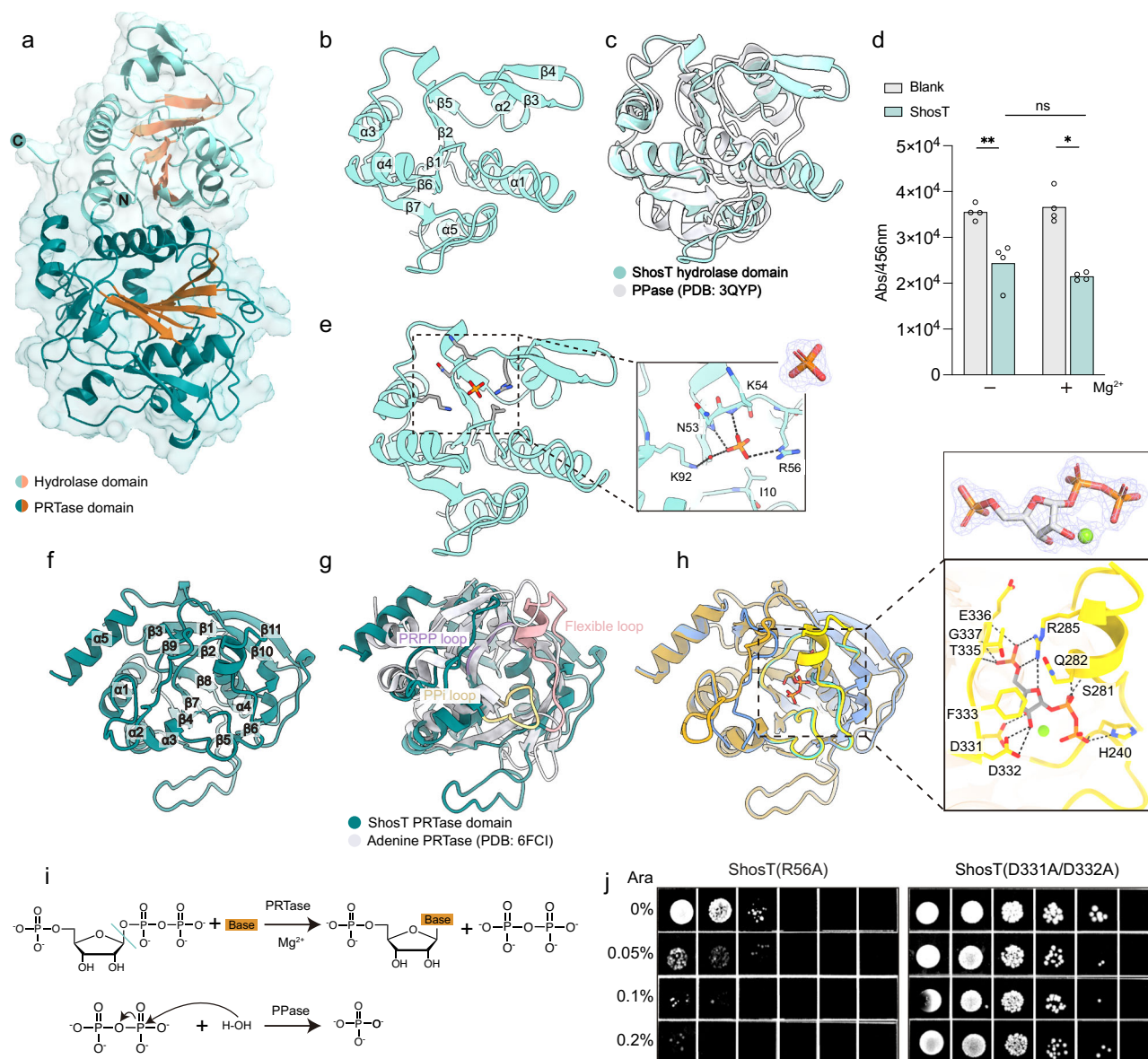
Fig. 2 | Structure and activities of ShosT. a Crystal structure of ShosT. The N- and C-termini of ShosT are indicated. The central β-sheets of the two Rossmann-fold domains are colored orange. **b** Structure of ShosT hydrolase domain. The secondary structures are labeled. **c** Superimposition of ShosT hydrolase domain and *Bacteroides thetaiotaomicron* PPase. **d** PPase activity of purified ShosT by measuring the absorbance of PPi. Bar graphs represent the mean of four replicates with individual data points overlaid. **P = 0.0045, *P = 0.0286, calculated by two-tailed Student's *t* test. Source data are provided as a Source Data file. **e** Structure of ShosT hydrolase domain complexed with phosphate. The details of the phosphate binding are shown in the enlarged part. The electron density map of phosphate (Fo-Fc omit map, contoured at 3 σ) is shown. **f** Structure of ShosT PRTase domain. The secondary structures are labeled. **g** Superimposition of ShosT PRTase domain and human APRT. **h** Superimposition of ShosT PRTase-PRPP (orange) and PRTase alone (blue). PRPP-binding loops are colored yellow and green in the PRTase-PRPP and PRTase alone structures, respectively. The details of the PRPP binding are shown in the enlarged part. The electron density map of PRPP and the bound Mg^{2+} (Fo-Fc omit map, contoured at 3 σ) is shown. **i** The enzymatic functions of PRTase and PPase. **j** Representative plating assay showing the cell toxicity of the indicated ShosT mutants. The arabinose concentrations used for inducing are indicated.

Since no external phosphate molecules were introduced during protein purification and crystallization, this hydrolysis product of PPi confirmed again the pyrophosphatase activity of ShosT. In the ShosT-PO_4^{3-} structure, the phosphate anion formed hydrogen bonds with the side-chain of R56 and the main-chains of N53 and K54, and interacted with K92 via water molecules (Fig. 2e).

The C-terminal PRTase domain of ShosT also adopted a typical Rossmann fold composed of a central five-stranded β-sheet (β1-β2-β8-β7-β4) sandwiched by two layers of α helixes (Fig. 2f). Structural analysis indicated a high similarity to adenine phosphoribosyltransferase (APRTase) (Fig. 2g), which is essential for purine homeostasis in

prokaryotes and eukaryotes[18]. Phosphoribosyltransferase proteins are known to catalyze the transfer of a phosphoribosyl group from 5-phosphoribosyl-1-pyrophosphate (PRPP) to a base, leading to the formation of a nucleoside monophosphate[19]. The C-terminal PRTase domain of ShosT contained the three typical PRPP-binding loops: the 'PPi loop' between β4 and α3, the 'flexible loop' between β8 and α4, and the 'PRPP loop' between β6 and α5[18,20] (Fig. 2g). Compared to APRTase, ShosT's PRTase domain had a much longer flexible loop (Fig. 2g).

To evaluate the PRTase activity of ShosT, we checked the interaction between ShosT and a variety of purines and the shared substrate
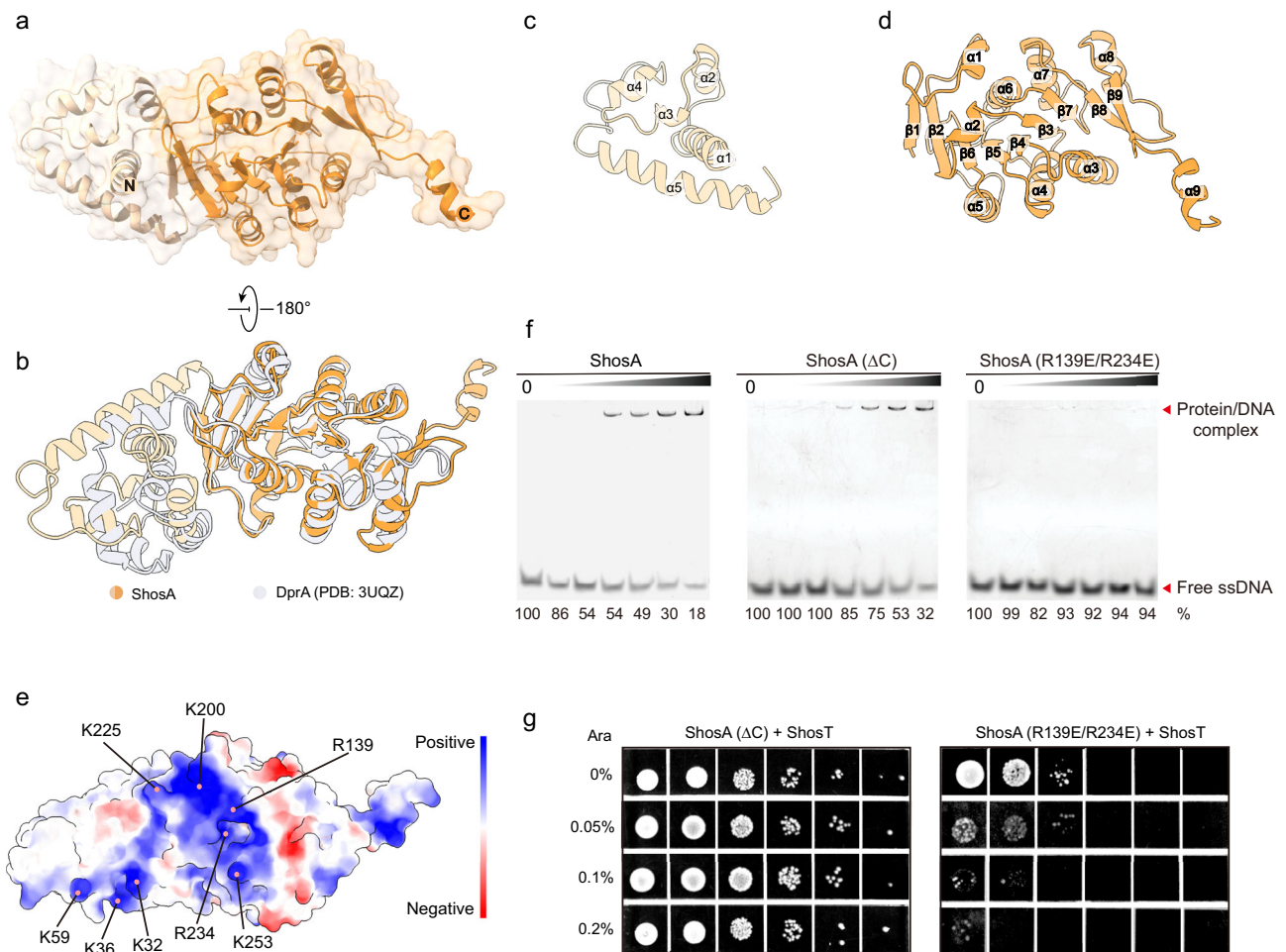
Fig. 3 | Structure and activities of ShosA. a Crystal structure of ShosA C-terminal truncation. The SAM and DprA domains are colored in light orange and orange. **b** Superimposition of ShosA and *Streptococcus pneumoniae* DprA. **c** Structure of ShosA SAM domain. **d** Structure of ShosA Rossmann-fold domain. **e** The electro-static surface potential of ShosA. Blue and red (±5 kT/e) indicate the positively and negatively charged areas of the protein, respectively. **f** ShosA binds ssDNA in vitro.

Electrophoretic mobility shift assay is performed using 5′ Cy3-labeled 54-nt ssDNA. Different concentrations of ShosA proteins (from 0 to 0.8 µM) were incubated with 0.1 µM DNA. Percent of the free DNA is calculated based on the gray scanning analysis. This experiment is repeated three times independently with similar results. **g** Representative plating assay showing the ShosT toxicity with indicated ShosA mutants. The arabinose concentrations used for inducing are indicated.

PRPP, using differential scanning fluorimetry (DSF). The results showed that ShosT bound to PRPP but exhibited no binding activity towards any tested purines (Supplementary Table 1). We then determined the crystal structure of ShosT-PRPP complex. Compared to the disordered conformation in the apo structure, the flexible loop of ShosT's PRTase domain formed a short alpha helix in the presence of PRPP (Fig. 2h), implying the PRPP binding stabilized the conformation of the flexible loop. All the three PRPP-binding loops were involved in the interaction of PRPP (Fig. 2h). Especially, the flexible loop formed hydrogen bonds with all the three moieties of PRPP (5′-phosphate, ribosyl group and PPi group) (Fig. 2h).

The fusion of the PPase and PRTase domains in ShosT implied a close functional association of these two domains. The PRTase catalyzes the transference of the ribose-5′-phosphate group from the substrate PRPP to a specific ligand, while the generated product PPi is subsequently hydrolyzed by the PPase, driving this reaction forward (Fig. 2i). To confirm the cooperation of these two domains, we introduced specific point mutations to disrupt the active site of the PPase or the PRTase. The PRTase mutant (D331A/D332A) completely abolished the cell toxicity, while the PPase mutant (R56A) only marginally reduced the cell toxicity (Fig. 2j), indicating that the PRTase played a dominant role to mediate cell death, and the PPase positively regulated the PRTase-mediated cell death.

Crystal structure and DNA-binding of ShosA

To provide insights of ShosA's function in neutralizing toxicity, we determined the crystal structure of a ShosA truncation (residues 1–313, excluding the C-terminal disordered loop) at 2.0-Å resolution (Fig. 3a). The purified full-length ShosA was unstable and inclined to precipitate, while the C-terminal truncation of ShosA was stable (Supplementary Fig. 1).

Structural comparison showed that ShosA had a clear homology with DNA processing protein A (DprA), a widespread bacterial protein that binds single-stranded DNA (ssDNA) and assists RecA loading for homology-directed natural chromosomal transformation[21] (Fig. 3b).

ShosA adopted a two-domain architecture: an N-terminal sterile alpha motif (SAM) domain (residues 1-94) and a C-terminal Rossmann-fold domain (residues 95-313) (Fig. 3a). The SAM domain is composed of five α-helices (Fig. 3c), and the Rossmann-fold domain consisted of a central extended nine-stranded β-sheet and nine flanking α-helices (Fig. 3d). An extensive positive-charged region was observed on ShosA's surface (Fig. 3e), implying a DNA-binding function. The DprA family is known as DNA-binding proteins with a preference for ssDNA[21]. We thus evaluated the DNA-binding ability of the ShosA and its mutants (C-terminal truncation or charge reversal mutations) by electromobility shift assay (EMSA). Both wild-type ShosA and its C-terminal truncated mutant showed ssDNA-binding ability, while the
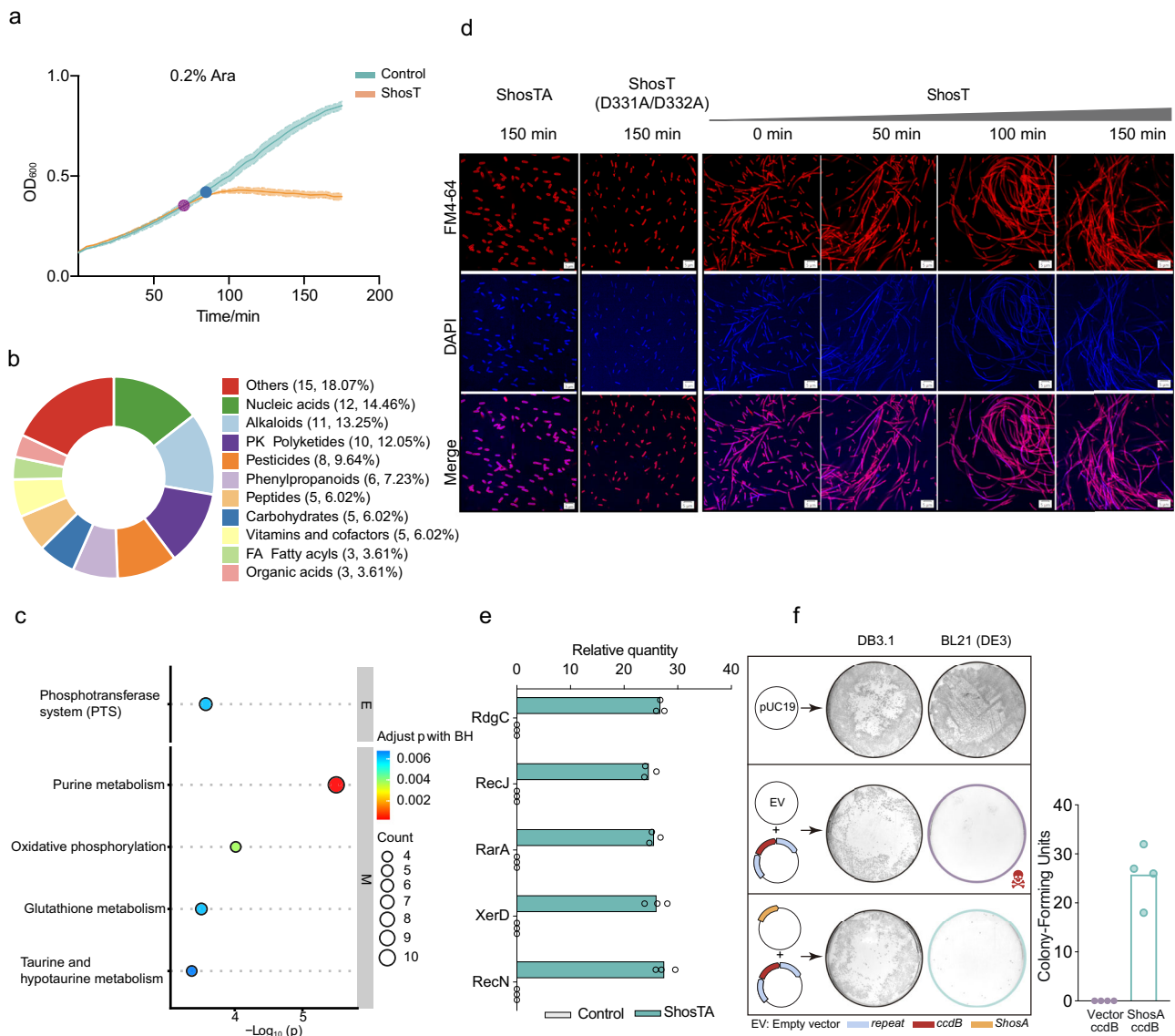
Fig. 4 | The mechanisms for ShosT-mediated toxicity and ShosA-mediated anti-toxicity. a Cell growth curves of *E. coli* BL21(DE3) strain expressing ShosT. Empty vector is used as the control. Results of three experiments are presented as the average of three replicates with shaded areas indicating SD. The time points of the drop of cell growth (blue) and cell collection (purple) are marked. Source data are provided as a Source Data file. **b** Diagram of the differential metabolite classification (KEGG). **c** Bubble map of KEGG pathway enrichment (up to top 5). **d** Fluorescence microscopy of *E. coli* BL21(DE3) cells expressing the whole system ShosTA, ShosT inactive mutant (D331A/D332A) or wild type ShosT. This experiment is repeated three times independently with similar results. Scale bars: 5 μm. **e** IP-MS/MS analysis reveals in vivo interactions between ShosA and some recombination-associated proteins. FLAG-tagged ShosA in the context of the full ShosTA system or FLAG-tag alone are used. Bar graphs represent the mean of three replicates with individual data points overlaid. **f** ShosA rescues *E. coli* BL21(DE3) cells from the toxicity of *ccdB*. Left, representative plating assay for indicated plasmids. Right, quantification of the left panel. Bar graphs represent the mean of four replicates with individual data points overlaid. Source data are provided as a Source Data file.

charge reversal mutant failed to bind ssDNA (Fig. 3f). ShosA also bound to dsDNA, albeit with a lower binding capability than that to ssDNA (Supplementary Fig. 2).

Then we validated the toxin-neutralizing ability of ShosA mutants by colony forming assay. The C-terminal truncation of ShosA showed no effect on its toxin-neutralizing ability, whereas the charge reversal mutant significantly increased the cell toxicity (Fig. 3g). These results indicated that the DNA-binding capability of ShosA played an essential role in neutralizing the cell-toxicity of ShosT.

ShosT interferes purine metabolism to impair genome replication

To elucidate the mechanism of the cell toxicity of ShosT, we performed untargeted metabolomics to identify the host metabolic pathways affected by ShosT. To ensure that the changes of metabolome are solely from the toxin ShosT instead of subsequent cell death, we harvested the cells 10 min before the drop of cell growth mediated by the toxicity of ShosT (Fig. 4a). The differential metabolites in the control and the ShosT-expressing samples were mapped to the KEGG database, and the classification analysis showed that the major differential metabolites were nucleic acid (14.46%) and alkaloids (13.25%), the potential products and substrates of ShosT PRTase, respectively (Fig. 4b). Further analysis of the metabolic pathways of the differential metabolites by KEGG pathway enrichment revealed that the predominant effect of ShosT is exerted on purine metabolism (Fig. 4c), indicating the cell toxicity of ShosT was mediated by interfering the purine metabolism. Although xanthine is among the top 30 differential metabolites (Supplementary Fig. 3), no
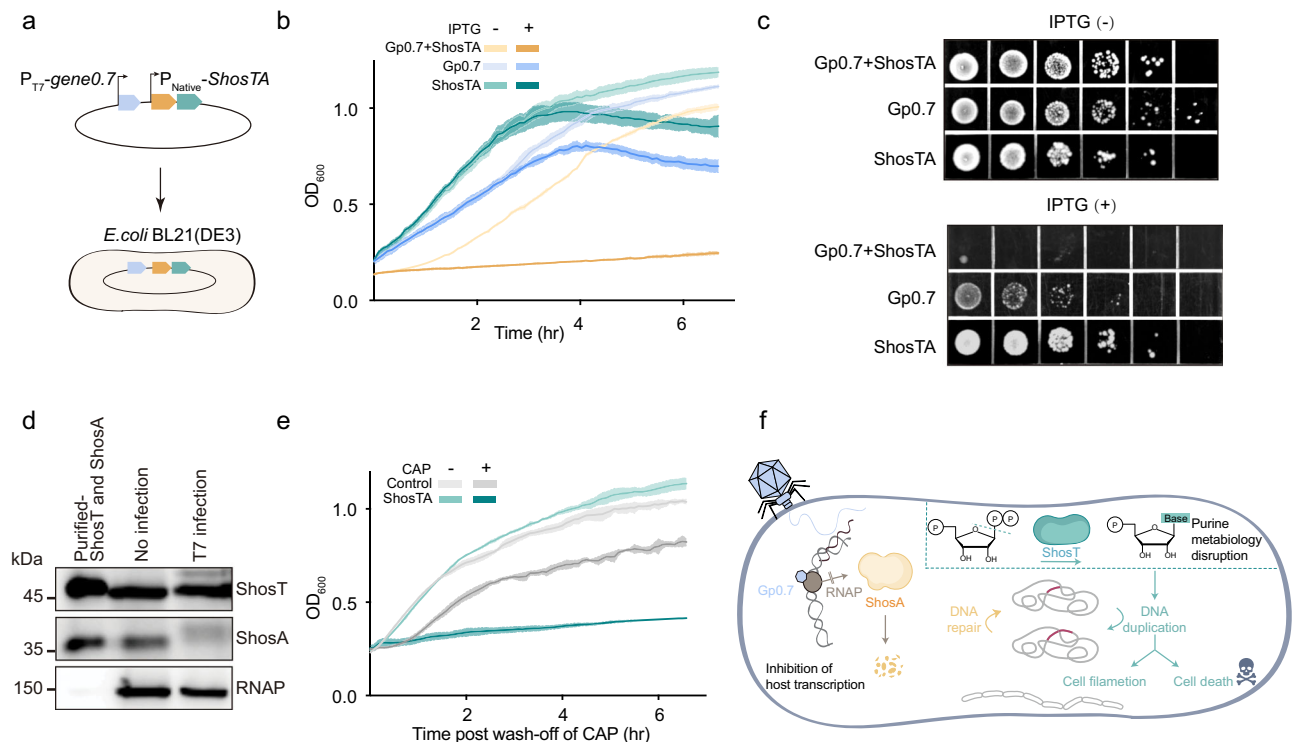
Fig. 5 | Phage Gp0.7 triggers the immunity mediated by ShosTA. a Schematic diagram of the co-expression assay for Gp0.7 and ShosTA. b Co-expression of Gp0.7 and ShosTA results in cell death. Growth curves for *E. coli* BL21(DE3) cells expressing indicated proteins are shown. Results of three experiments are presented as the average of three replicates with shaded areas indicating SD. c Representative plating assay shows that co-expression of Gp0.7 and ShosTA induces cell death. d The protein levels of ShosT and ShosA upon phage infection measured by western blot. RNAP is used as the loading control. This experiment is repeated three times independently with similar results. e Growth curves for *E. coli* BL21(DE3) cells treated with chloramphenicol (CAP) for 30 min. Results of three experiments are presented as the average of three replicates with shaded areas indicating SD. The presence of ShosTA results in significant cell death. f Model for the anti-phage mechanism of ShosTA system. Source data are provided as a Source Data file.

interaction between ShosT and xanthine was detected (Supplementary Table 1).

Purine metabolism plays an important role in nucleic acid synthesis, and the disruption of cellular nucleotide pools will result in DNA damage and cell filamentation in bacteria[22,23]. We then evaluated whether ShosT induced cell filamentation and DNA damage. Visualized by fluorescence microscopy, the ShosT-expressing *E. coli* cells showed a progressively filamentous morphology while the ShosT PRTase inactive mutant (D331A/D332A) did not induce cell filamentation (Fig. 4d). Genome sequencing data showed that the ShosT-expressing cells accumulated significant DNA duplications (Supplementary Fig. 4 and Supplementary Table 2).

In summary, these results indicated that ShosT disrupted purine metabolism to impact the nucleotide pool, subsequently destabilized the genome via creating DNA duplications, and ultimately resulted in cell death.

ShosA helps eliminate the genome duplications

ShosA contains a SAM domain which usually participates in protein-protein interaction[21]. To probe the possible ShosA interacting proteins, we expressed C-terminally FLAG-tagged ShosA in the context of the full ShosTA system or FLAG-tag alone and performed immunoprecipitation followed by tandem mass spectrometry (IP-MS/MS). Five recombination-associated proteins, including RdgC[24], RecJ[25], RarA[26], XerD[27] and RecN[28], are among the significantly enriched proteins in the ShosA pulldown sample (Fig. 4e). Notably, these five recombination-associated proteins are not detected in the control samples.

Homologous recombination is a type of genetic recombination in which nucleotide sequences are exchanged between two similar or identical molecules of DNA. The interactions between ShosA and recombination-associated proteins implied a close functional association between ShosA and DNA recombination. We thus proposed that ShosA might eliminate the ShosT-induced genome duplications by homologous recombination to neutralize ShosT's toxicity.

To evaluate this hypothesis, we designed a construct containing a toxin gene *ccdB* placed in between two repeat sequences (Fig. 4f). Here, *ccdB* is used as a death reporter. This construct was replicated in the *E. coli* strain DB3.1 that tolerates the expression of the toxin gene. However, normal *E. coli* strains, such as BL21(DE3), will not survive unless the toxin gene *ccdB* is removed. We found that ShosA could rescue some BL21(DE3) cells from the toxicity of *ccdB* (Fig. 4f), indicating that ShosA may promote the deletion of the toxin gene *ccdB* via homologous recombination. The reason why only some BL21(DE3) cells were rescued is probably that the survival of a BL21(DE3) cell needs the elimination of all the copies of *ccdB* gene while the efficiency of ShosA is not high enough.

Identification of the phage triggers for ShosTA defense system

A previous study has identified three mutated genes (*gene2.5*, *gene0.7* and *gene4*) from escaper T7 phage for ShosTA defense system, encoding ssDNA-binding protein (SSB), inhibitor of host RNA polymerase (Gp0.7) and primase-helicase, respectively[29]. However, these potential phage triggers have not been verified yet. Among the escape T7 mutants, SSB and Gp0.7 are most frequently mutated[29]. To explore whether SSB or Gp0.7 activates ShosTA system, we co-expressed ShosTA and SSB or Gp0.7 in *E. coli* and monitored the cell growth (Fig. 5a–c and Supplementary Fig. 5). Co-expression of T7 SSB and ShosTA did not show significant cell toxicity (Supplementary Fig. 5),

while co-expression of T7 Gp0.7 and ShosTA resulted in a complete cell death (Fig. 5b). The results of plating assay also confirmed that T7 Gp0.7 induce acute cell toxicity for the ShosTA-containing cells (Fig. 5c). These results indicated that Gp0.7 triggered the abortive infection function of ShosTA defense system.

In the co-expression assay (Fig. 5a), we observed an interesting phenomenon we made. We used *E. coli* strain DH5α to do cloning of the co-expression construct of Gp0.7 and ShosTA. We found that some colonies were obviously larger than others. Sequencing of the plasmids extracted from these larger colonies exhibited deletion mutations within *gene0.7*, without exception. Analysis of these deletion mutations showed that the deletions occurred between some repeat segments within *gene0.7* (Supplementary Fig. 6), suggesting that ShosA removed these repeats by homologous recombination. This is in line with our finding that ShosA promoted homologous recombination (Fig. 4f). Notably, 6-8 bp repeats were sufficient for the occurrence of the ShosA-mediated homologous recombination (Supplementary Fig. 6).

A typical TA system contains a stable toxin and a cognate unstable antitoxin[2]. ShosA, the antitoxin of ShosTA system, also had intrinsic instability endowed by its C-terminus (Supplementary Fig. 1). Previous studies have discovered that Gp0.7 of T7 is involved in accomplishing shutoff of the host *E. coli* RNA polymerase activity by phosphorylating the host RNA polymerase (RNAP) during the early stages of infection[30,31]. Thus, Gp0.7 might induce the transcription shutoff to hinder the continuous synthesis of the antitoxin ShosA and subsequently release the toxicity of ShosT. The quantitative PCR (qPCR) results confirmed that phage infection or expression of Gp0.7 suppressed the transcription of ShosTA system (Supplementary Fig. 7). We then checked the protein levels of ShosT and ShosA during phage infection. Western blotting results showed that ShosT protein remained generally constant before and after phage infection while the protein level of ShosA significantly decreased after phage infection (Fig. 5d). To confirm that the modulation of host translation plays a role in the activation of ShosTA defense system, we used an antibiotic, chloramphenicol, to transiently inhibit host protein synthesis. The transient treatment of chloramphenicol exhibited dramatic cell toxicity for the cells harboring ShosTA system compared to the ShosTA-deficient cells (Fig. 5e). Treatment with rifampicin, an inhibitor of the microbial RNAP, to transiently inhibit host transcription resulted in significantly longer times for the ShosTA-containing cells to recover (Supplementary Fig. 8). These results support a model in which phage Gp0.7 triggers the toxicity of the ShosTA system by transcription shutoff coupled to intrinsically fast antitoxin turnover.

Together, our results suggest ShosTA is a type IV TA system consisting of an antitoxin protein that indirectly antagonizes the enzymatic activity of its cognate toxin. We propose a model for the mechanism action of ShosTA anti-phage system (Fig. 5f). ShosT represents a toxin which interferes with purine metabolism to induce DNA duplication, cell filamentation and cell death. ShosA facilitates DNA damage repair to antagonize ShosT. Upon infection, phage-mediated inhibition of host transcription induces the shutoff of the synthesis of ShosT and ShosA. The instability of ShosA then results in down-regulation of the antitoxin's protein level and releasing the cell toxicity of the existing toxin ShosT.

Discussion

The notion that TA systems may function in anti-phage defense provides an explanation for their widespread distribution in bacteria. Here we explore an anti-phage TA system ShosTA, elucidate the structures and enzymatic activities of ShosT and ShosA, and propose a mechanism how this defense system detects phage infection and provide defense against phages.

Since expression of ShosT resulted in acute cell toxicity (Fig. 1d), we obtained ShosT protein by co-expression with ShosA. However, no

strong interaction between ShosT and ShosA has been detected. Thus, the ShosTA system represented a type IV TA system in which the toxin and antitoxin are proteins and the antitoxin counteracts the toxin without direct interaction[6].

It has been proposed that disruption of nucleotide pools is a successful antiviral defense strategy shared by eukaryotes and prokaryotes[32]. Here we showed that ShosT, the PRTase-containing toxin, impacted on purine metabolism and induced DNA duplication, cell filamentation and cell death (Fig. 4). Thus, ShosT would likely disrupt the DNA replication for both bacterial cell and phage. Since the phage replication cycle would be halted, it is not necessary for the infected bacterial cell to commit suicide so quickly. This provides an explanation for the lack of the earlier culture collapse for ShosTA-containing cells at the high-MOI infection (Fig. 1c).

The PRTase domain has been proposed as a toxin in RqlHI TA system, resulting in cell filamentation[33]. Besides ShosTA and RqlHI, the cellular morphological change into a filamentous form is also observed in other TA systems, such as ParDE[34], AvcID[35,36] and ccdAB[37]. One shared feature among these TA systems is that their toxins cause DNA damage through various mechanisms.

Although no PRTase activity has been observed for ShosT against four common purines, we have showed that ShosT binds the common substrate PRPP (Fig. 2h & Supplementary Table 1). Given that PRTases contribute to different metabolic pathways including purine and pyrimidine nucleotide biosynthesis, NAD(P)+ biosynthesis, and tryptophan biosynthesis, which crosstalk with each other by sharing PRPP as the sugar donor[38], the physiological substrates of ShosT may be other types of purine or pyrimidine, their derivatives, or intermediates.

However, several questions remain open. Further studies are needed to discover the detailed mechanisms of ShosT-mediated cell toxicity and ShosA-mediated homologous recombination, such as what are the physiological substrates of ShosT, what effector proteins ShosA recruits and how they co-operate to eliminate the DNA duplications. Notably, we could not exclude the possibility that ShosA somehow prevents the occurrence of the DNA duplications.

Collectively, our study reveals a distinct mechanism of action of a novel TA system ShosTA, and demonstrates that T7 phage Gp0.7 triggers the activation of ShosTA defense system. Furthermore, understanding the mechanisms that ShosTA system employs, such as the ShosT-induced genome duplication and the ShosA-mediated homologous recombination, may unveil molecular tools for DNA and genome manipulation.

Methods

Ethics statement

The 6–8 weeks old female BALB/c mice were supplied by Jiangsu Jicuiyaokang Animal Cultivation Farm (Nanjing, China). Animal experiments were performed following the protocol approved by the Biomedical Ethics Committee of the West China Hospital, Sichuan University. Ethical approval was given by the West China Hospital of Sichuan University Laboratory Animal Ethics Committee (approval number 20240301035).

Bacterial strains and growth conditions

Escherichia coli strains were routinely grown at 37 °C in Luria broth (LB) with shaking. Whenever applicable, media were supplemented with ampicillin (100 µg mL⁻¹), kanamycin (50 µg mL⁻¹), or streptomycin (50 µg mL⁻¹) to ensure the maintenance of plasmids.

Phage cultivation and plaque assays

Phages were purchased from Deutsche Sammlung von Mikroorganismen und Zellkulturen (DSMZ): T2 (DSM 16352), T4 (DSM 4505), T5 (DSM 16353), T7 (DSM 4623) and P1 (DSM 5757). Phages were propagated by picking a single phage plaque into a liquid culture of *E. coli* BL21(DE3) at an OD$_{600}$ of 0.2–0.4 until culture collapse. Propagated

phage lysates were centrifuged for 10 min at 4000 rpm to pellet bacterial cells and the supernatant was filtered through a 0.2-μm filter. Phage titer was determined by small drop plaque assay.

The ShosTA system or its mutant was cloned into pJET1.2 vector (Thermo Fisher) under its native promoter. E. coli BL21(DE3) cells containing pJET1.2-ShosTA or empty pJET1.2 vector were grown in LB for 6 h at 37 °C. Cultures were diluted 1:50 into fresh LB medium and grown until mid-logarithmic phase. Then 2 mL of the bacterial culture was mixed with 25 mL melted LB agar (LB + 0.6% agar) and left to dry for 1 h at room temperature. Tenfold serial dilutions in LB were performed for each of the tested phages and 3-μL drops were spotted on the solidified agar. After the drops dried up, the plates were inverted and incubated at 37 °C for 4 h (T7) or overnight (T2, T4, T5 and P1). Plaque forming units (PFUs) were determined by counting the derived plaques after incubation. Efficiency of plating (EOP) was calculated by comparing the ability of the phage to form plaques on an experimental strain relative to the control strain.

Phage-infection dynamics in liquid medium

Single colonies of E. coli BL21(DE3) with pJET1.2-ShosTA or pJET1.2 were grown in LB for 6 h at 37 °C. Cultures were diluted 50 times in fresh LB medium supplemented with ampicillin and incubated at 37 °C with shaking until early log phase. 180 μL of the early-log culture was transferred into wells in a 96-well plate containing 20 μL of either LB or phage T7 lysate for a final MOI of 2, 0.2 or 0.02. Infections were performed in duplicate from overnight cultures prepared from three separate colonies. Plates were immediately transferred to a plate reader Tecan Infinite 200 set to 37 °C with 4.5-mm orbital shaking and OD_{600} values were monitored every 5 min.

Toxicity assays on solid media

The arabinose-inducible vector pBAD (Thermo Fisher) and E. coli BL21-AI were used for toxicity assays. Single colonies containing pBAD-ShosTA or variants were cultured for 6 h at 37 °C in LB medium. After diluted 50 times with fresh LB medium and further 45-min growth, each culture was divided into four equal volumes and induced by 0.02%, 0.05%, 0.1% and 0.2% arabinose for 30 min. Cultures were then serially diluted tenfold with LB and spotted on LB + 0.6% agar plates supplemented with 0.02%, 0.05%, 0.1% and 0.2% arabinose, respectively. Plates were incubated at 37 °C overnight before imaging.

Protein expression and purification

The shosA gene (Escherichia coli APEC O1, GenBank: ABJ01487.1) was synthesized and cloned into a vector derived from pET-28a (+) (Novagen), which contains an N-terminal 6His-tag followed by a tobacco etch virus (TEV) protease recognition site and a linker (ASGSGTGSGS). The shosT gene (Escherichia coli APEC O1, GenBank: ABJ01488.1) was synthesized and cloned with a C-terminal 6His-tag following shosA and a ribosome binding site for co-expression. E. coli BL21 (DE3) was used for protein expression. Single colony of transformant was cultured overnight in 20 mL LB medium supplemented with kanamycin at 37 °C with shaking and diluted into 1 L LB medium. Protein expression was induced by 0.2 mM IPTG at 18 °C for 16 h. The cells were harvested by centrifugation and the cell pellets were resuspended in binding buffer (20 mM Tris–HCl pH 8.0, 500 mM NaCl, 10% glycerol). After lysis by an ultrahigh-pressure homogenizer, the supernatant was separated from the pellet by centrifugation and filtered through 0.45-μm filters. The resultant supernatant was collected and passed over a Ni^{2+} affinity column pre-equilibrated with binding buffer. Nonspecifically bound proteins were removed stepwise by binding buffer supplemented with 5 mM, 10 mM and 20 mM imidazole, and the target protein was eluted in binding buffer supplemented with 250 mM imidazole. The eluted proteins were buffer-exchanged to binding buffer and incubated with TEV protease to remove the N-terminal 6His-tag and then passed through a Ni^{2+} affinity column to remove free His tag, un-cleaved protein and TEV protease. The target proteins were further purified via a gel-filtration column (Superdex® 200 10/300 GL, GE Healthcare) previously equilibrated in a buffer consisting of 20 mM HEPES pH 7.4, 300 mM NaCl, 1 mM DTT. All the purified proteins were concentrated to ~15 mg mL^{-1} and stored at −80 °C until use.

Crystallization and X-ray structure determination

ShosA and ShosT were concentrated to ~15 mg mL^{-1} and crystallized by hanging-drop vapor diffusion method at 18 °C. The crystals of ShosA were grown in a buffer consisting of 18% PEG 2000, 0.1 M imidazole pH 7.0, 0.2 M ammonia citrate pH7.0. The crystals of ShosT were grown in a buffer consisting of 20% PEG 6000, 0.1 M MES pH 6.2. To obtain complex crystals, ShosT was incubated with PPi (10 mM) or PRPP (10 mM) for 1 h at 4 °C prior to crystallization, and crystals appeared in a buffer consisting 18–20% PEG 6000 and 0.1 M MES pH 6.0-6.5.

Crystals were immersed briefly in precipitant solution supplemented with 20% glycerol as cryoprotectant, and flash frozen in liquid nitrogen. Diffraction data were collected on beamline BL19U1 of National Facility for Protein Science Shanghai (NFPS) at Shanghai Synchrotron Radiation Facility. The data collected were processed by the HKL-3000[39]. Structures were determined by molecular replacement. Structure refinement and model building were performed with PHENIX[40] and Coot[41] iteratively. All models were validated with MolProbity[42]. Details of the data processing and refinement statistics were summarized in Supplementary Table 3. Images of representative electron density for each structure are provided in Supplementary Fig. 9.

Vaccination

Mouse polyclonal antibodies for ShosT and ShosA were generated by immunizing 8- to 10-week-old healthy female BALB/c mice with purified wild type ShosA or ShosT proteins. All mice were housed in SPF-grade facilities, cages with standard conditions (50% relative humidity and 12/12 h light-dark cycle) at 25 °C. Proteins were fully emulsified with an equal volume of Freund's Complete Adjuvant (Sigma) and injected into mouse hind limb muscles. Two weeks later, proteins were emulsified with an equal volume of Freunds Incomplete Adjuvant (Sigma) and injected into mouse hind limb muscles, then repeat in a fortnight. One week later, antiserum titer was measured by western blot using tail vein blood. The blood of mice was collected and centrifuged, then the serum containing polyclonal antibody was prepared.

Western blot

Overnight cultures of E. coli BL21(DE3) were diluted 100 times into a volume of 20 mL LB and grown for ~1 h to an OD_{600} of 0.3–0.5 before infection with T7 at MOI of 2. And the cells were harvested 15 min post infection by centrifugation for 20 min at 4000 rpm and resuspended in 500 μL 1×PBS. Samples were ultrasonic crushed for 10 min on ice and followed by 5 min centrifugation at 13,000 rpm to remove debris. Then samples were separated by 10% SDS-PAGE and transferred to PVDF membranes, which were blocked for 1 h in TBST (100 mM Tris pH 7.5, 150 mM NaCl, 0.1% Tween-20) with 5% milk at room temperature with shaking. Membranes were incubated with primary antibodies diluted in TBST buffer containing 5% BSA overnight at 4 °C. Antibody against E. coli RNA polymerase (Rabbit, 1:5000; Abcam) was used as loading control. Membranes were washed 3 times with 10 mL TBST then incubated with the appropriate combination of anti-rabbit HRP Conjugated Goat anti-Rabbit IgG (H + L) (1:50,000; HUABIO) or anti-mouse HRP Conjugated Goat anti-Mouse IgG (H + L) (1:20,000; HUABIO) secondary antibodies at 1:10,000 dilution in TBST for 1 h at 25 °C with shaking. Membranes were again washed 3 times with 10 mL TBS, then incubated with ClarityTM Western ECL Substrate (Bio-Rad) for 2 min and imaged on Chemical Imaging System (Bio-Rad).

Antibiotic assay

Overnight cultures of E. coli harboring the ShosTA system or empty vectors were diluted 50 times in LB medium with 0.2% arabinose and cultured at 37 °C until OD_{600} ~ 0.3. Then the cultures were divided into equal volumes and supplemented with Chloramphenicol to a final concentration of $68 \mu g\,mL^{-1}$. Samples were incubated at 37 °C for 35 min, then centrifuged for 5 min at 4000 rpm and resuspended in 2 mL LB. 200 μL of the samples were transferred into wells in a 96-well plate, which were immediately transferred to a plate reader Tecan Infinite 200 set to 37 °C with 4.5-mm orbital shaking and OD_{600} values were monitored every 5 min.

Electrophoretic mobility shift assays

The 1 μM ssDNA (54-nt with 5′Cy3) were incubated with purified ShosT, ShosA and $ShosA^{R134E/R243E}$ in CutSmart buffer (NEB) at 25 °C for 30 min. The final concentration of ssDNA and protein in a 10 μL mixture were 100 nM and 0–800 nM, respectively. Samples were analyzed by native polyacrylamide gels (6%) and visualized with Chemical Imaging System (Bio-Rad).

Fluorescence microscopy

Overnight cultures were diluted 50 times into LB supplemented with ampicillin. Cultures were grown to OD_{600} ~ 0.3 and sampled at 0, 50, 100, 150 min after L-ara induction. Samples were added 120 μL glutaraldehyde, allowed to fix for 5 min and centrifuged at 13,300 rpm for 3 min. Harvested samples were resuspended in 1 mL LB with $2 \mu g\,mL^{-1}$ DAPI (Sigma-Aldrich) and $1 \mu g\,mL^{-1}$ FM4–64 (Thermo Fisher Scientific) and stained for 20 min. Samples were washed with 1 mL LB and resuspended in 50 μL LB. Finally, 2 μL samples were spotted onto microscope slides. The signals of DAPI and FM4-64 were visualized and photographed using CF405 and CF561 (Olympus SpinSR10, a Leica DM5000b epifluorescence microscope).

Pyrophosphate hydrolysis assay

Pyrophosphate hydrolysis activity of ShosT was detected by measuring the decreasing of PP_i thought PhosphoWorks™ Fluorimetric Pyrophosphate Assay Kit (AAA bioquest). The reactions were performed using 1 μM ShosT and 100 μM standard PP_i in a buffer containing 20 mM HEPES pH 7.4, 300 mM NaCl, 1 mM $MgCl_2$, 0.5 mM DTT. The reactions were incubated at room temperature for 30 min and then incubated with a fluorogenic PPi sensor for another 30 min. The fluorescence intensity was measured ($\lambda ex = 316$ nm and $\lambda em = 456$ nm) using a plate reader Tecan Infinite 200. A T test with a two-tailed distribution was applied to evaluate the significance of changed pyrophosphate.

Differential scanning fluorimetry (DSF) assays

The thermal stability of wild type ShosT protein was analyzed using Bio-Rad CFX Connect™ Real-Time System to image 96-wells simultaneously. The protein was diluted to $0.2\,mg\,mL^{-1}$ in 20 mM HEPES pH 7.4, 300 mM NaCl and 1 mM DTT supplemented with 500 μM PRPP, purines, or pyrimidines and incubated at room temperature for 30 min. A volume of 200 μL per well was used in plates and the protein solution was gradually increased from 30 to 95 °C at 0.01 °C per sec with 16 acquisitions per degree. The protein stability was assessed by measuring the fluorescence of a reporter dye, SYPRO orange (Thermo Fisher Scientific), diluted 1,000-fold. Each experiment was performed in triplicate in order to compute the mean value of the thermal melting (Tm) profile and its standard deviation.

Untargeted metabolomics

Early-log cultures of BL21(DE3) harboring pBAD-ShosT or empty vector were induced by 0.2% L-ara and cultured at 37 °C with shaking. Samples were collected 10 min before cell growth arrest (about 80 min after inducing). The metabolites were extracted from cells with 1 mL precooled methanol/acetonitrile/water (v/v, 2:2:1) under sonication for 1 h in ice baths, incubated at −20 °C for 1 h followed by centrifugation at $14,000 \times g$, 4 °C for 20 min. The supernatants were recovered and concentrated to dryness in vacuum. Five biological replicates were made for each sample.

Metabolomics profiling was analyzed by UPLC-ESI-Q-Orbitrap-MS system (UHPLC, Shimadzu Nexera X2 LC-30AD, Japan) coupled with Q-Exactive Plus (Thermo Fisher Scientific, USA). For liquid chromatography (LC) separation, samples were analyzed using a ACQUITY UPLC® HSS T3 column (2.1×100 mm, 1.8 μm) (Waters, USA) at 40 °C. The mobile phase A: 0.1% formic acid aqueous solution, B: acetonitrile. The gradient elution program was as follows: 0–2 min, 0% buffer B; 2-6 min, 0% to 48% buffer B; 6–10 min, 48–100% buffer B; 10–12 min, 100% buffer B; 12–12.1 min, 100–0% buffer B; 12.1–15 min, 0% buffer B. The flow rate was set to 0.3 mL/min and the sample injection volume was 4 μL. Both electrospray ionization (ESI) positive-mode and negative mode were applied for MS data acquisition. The ESI source conditions were set as follows: Spray Voltage: 3.8kv (+) and 3.2kv (−); Capillary Temperature: 320 (±); Sheath Gas: 30 (±); Aux Gas: 5 (±); Probe Heater Temp: 350 (±); S-Lens RF Level: 50. MS acquisition time: 15 min. In MS acquisition, the instrument was set as follow: ion scan range: 70–1050 m/z; MS resolution: 70,000 @ m/z 200; AGC target: 3e6; Maximum IT: 100 ms. The MS/MS acquisition was performed as follows: each full scan was triggered to acquire MS/MS spectra of the 10 highest intensity MS ions, MS/MS resolution: 17,500 @ m/z 200; AGC target: 1e5; Maximum IT: 50 ms; Activation Type: HCD, Isolation window: 2 m/z, Stepped normalized collision energy: 20, 30, 40.

The raw MS data were processed using MS-DIAL for peak alignment, retention time correction and peak area extraction. In the extracted-ion features, only the variables having more than 50% of the nonzero measurement values in at least one group were kept. Data were mean-centered using Pareto scaling. Models were built on principal component analysis (PCA), orthogonal partial least-square discriminant analysis (PLS-DA) and partial least-square discriminant analysis (OPLS-DA). The discriminating metabolites were obtained using a statistically significant threshold of variable influence on projection (VIP) values obtained from the OPLS-DA model and two-tailed Student's t test (p value) on the normalized raw data at univariate analysis level. The p value was calculated by one-way analysis of variance (ANOVA) for multiple groups analysis. Metabolites with VIP values greater than 1.0 and p value less than 0.05 were statistically significant metabolites. Fold change was calculated as the logarithm of the average mass response (area) ratio between two arbitrary classes.

To identify the perturbed biological pathways, the differential metabolite data were performed KEGG pathway analysis using KEGG database (http://www.kegg.jp). KEGG enrichment analyses were carried out with the Fisher's exact test, and false discovery rate (FDR) correction for multiple testing was performed.

Genome sequencing and analysis

The genomic DNA of E. coli BL21(DE3) containing ShosT or empty vector was extracted by cetyl-trimethyl-ammonium-bromide (CTAB) based method. The DNA quality and quantify were determined by Qubit Flurometer (Invitrogen) and NanoDrop Spectrophotometer (Thermo Fisher Scientific), respectively. DNA-seq library was prepared by TruSeq Nano DNA Library Prep Kit (Illumina) using 1 μg of DNA. After trimming, reads were mapped to the reference genome sequence using BWA MEM software[43] under default mapping parameters. Copy number variations (CNVs) in the whole genome were analyzed by CNVnator (version 0.2.7)[44].

Immunoprecipitation and LC-MS/MS

Overnight cultures of ShosA-FLAG and FLAG alone cells were back-diluted in 50 mL LB and grown at 37 °C to an OD_{600} of 0.3 and then

induced with 0.2 mM IPTG. At 80 min post-induction 50 mL of sample was pelleted by centrifugation at $4000 \times g$ for 5 min. Pellets were decanted and resuspended in 1 mL of lysis buffer (20 mM Tris-HCl, 150 mM NaCl, 5% glycerol, 1 mM PMSF). Additional lysis buffer was added to samples to normalize sample concentrations by OD_{600}. Samples were ultrasonic crushed for 10 min in ice water and spun at $12,000 \times g$ for 10 min at 4 °C to pellet any debris. For each sample, 50 μL of Anti-FLAG magnetic beads (Smart-Lifescience) was mixed with 200 μL of lysis buffer and then collected to the side of the tube using a magnetic rack. Beads were then washed twice with 500 μL of lysis buffer. After the final wash, beads were mixed with 1 mL of sample and incubated for 20 min at 4 °C on an end-to-end rotor, and then washed in wash buffer (20 mM Tris-HCl, 150 mM NaCl, 1 mM PMSF) for three times. Beads were boiled to denature protein and run on SDS−PAGE. Each lane from the gel was excised. Proteins were reduced with 10 mM dithiothreitol (Sigma) for 1 h at 55 °C and then alkylated with 55 mM iodoacetamide (Sigma) for 1 h at 25 °C in the dark. Proteins were then digested with 10 ng μL^{-1} modified trypsin (Promega) at 37 °C overnight. Peptides were extracted by 50% acetonitrile/5% tri-fluoroacetic acid, followed by 75% acetonitrile/0.1% trifluoroacetic acid, and then incubated with 100% acetonitrile. Peptides were desalted using C18 Columns (Milipore) and then lyophilized. Three biological replicates were made for each sample.

The desalted peptides were resuspended in 0.1% formic acid. Peptides were separated on a C18 column (Dr. Maisch, Ammerbuch) and measured via LC-MS/MS using EASY-nLC 1200 system coupled to an Orbitrap Exploris 480 mass spectrometer (Thermo Fisher Scientific). Mass spectra were recorded with a mass range of 350 to 1800 m/z, a resolution of 60,000 with the automatic gain control (AGC) target of 300%. The MS raw data was analyzed with the software Maxquant version 1.6[45]. The protein label-free quantification (LFQ) reports of Maxquant were further processed in Perseus version 1.6.14[46]. The parameter settings were as follows: parent ion mass deviation set to less than 10 ppm, fragment ion mass deviation set to less than 0.02 Da, the database used is the *E. coli* protein sequence database, the minimum peptide length was set to 6 amino acids, the maximum peptide mass was set to 12,000 Da, Carbamidomethylation of cysteine was assigned as a fixed modification. Oxidation of methionine and protein N-terminal acetylation were assigned as variable modifications. Two missed trypsin cleavages were allowed. The false discovery rate (FDR) for both peptides and proteins was set to less than 1%, and the quantification method was label-free. Match between runs was enabled. The protein LFQ intensities were $\log_2$ transformed as relative quantity. A T-test with a two-tailed distribution was applied to evaluate the significance of proteins with changed abundance.

Bacterial growth upon induction of phage genes
The pCDF-Dute plasmid contains the phage gene under an inducible T7 promoter and ShosTA under native promoter. The phage gene or ShosTA alone as negative control. The plasmids were transformed into BL21(DE3). The toxicity of the phage genes was measured quantitatively by counting the number of bacterial colony-forming units (CFUs) per mL formed and growth curves after inducing expression of the phage gene overnight.

Single colony of transformant was cultured overnight at 37 °C with shaking. For CFUs, 3- μL drops of ten-fold serial dilutions of the overnight culture were spotted on LB agar plates with or without inducer (0.5 mM IPTG). Plates were incubated overnight at 37 °C and bacterial colonies imaged and counted. For growth curves, 180 μL of early-log culture was transferred into wells in a 96-well plate containing 20 μL of 0.5 mM IPTG, which were immediately transferred to a plate reader Tecan Infinite 200 set to 37 °C with 4.5-mm orbital shaking and OD_{600} values were monitored every 5 min.

Quantitative PCR
Bacterial cells containing the ShosTA system were infected by T7 phages with an MOI of 5 for 10 min. Gp0.7 were induced by IPTG for 30 min. The total RNA was extracted by Vazyme Bacteria RNA Extraction Kit (Vazyme). The reverse transcription was performed by PrimeScript RT Reagent Kit (TaKaRa), using 500 ng RNA as templates. Each PCR reaction included 1 μL cDNA, 2 μM ShosTA primers or 16 s RNA primers, and 1× AceQ Universal SYBR qPCR Master Mix (Vazyme). A CFX Connect Real-Time System (Bio-Rad) was used to amplify the cDNA templates. Melt curves were generated to confirm homogenous products by exposing samples to a final temperature gradient of 65−95 °C. The host-specific gene 16S RNA was used to normalize the quantity of the ShosTA gene. All the experiments have three replicates.

Statistics & reproducibility
Statistical analysis was performed using the GraphPad Prism 8 Software. Two-tailed Student's t test was used to compare differences. Significance level was set at $P > 0.05$. All values were reported as means ± s.d. The exact number of replicates and statistical tests are indicated in the figure legends.

Reporting summary
Further information on research design is available in the Nature Portfolio Reporting Summary linked to this article.

Data availability
Atomic coordinates and structure factors generated in this study have been deposited in the Protein Data Bank (PDB) under accession codes 8ZVA (ShosA), 8ZVB (ShosT), 8ZVD (ShosT-PO$_4^{3}$), and 8ZVC (ShosT-PRPP-Mg^{2+}). The sequencing raw data generated in this study have been deposited to Genome Sequence Archive (GSA) under accession code CRA019192. The protein mass spectrometry raw data generated in this study have been deposited to ProteomeXchange under accession code IPX0009810000. The metabolomics mass spectrometry raw data generated in this study have been deposited to MetaboLights under accession code MTBLS11212. Source data are provided with this paper.

References
1. Yamaguchi, Y., Park, J. H. & Inouye, M. Toxin-antitoxin systems in bacteria and archaea. *Annu Rev. Genet* **45**, 61–79 (2011).
2. Jurenas, D., Fraikin, N., Goormaghtigh, F. & Van Melderen, L. Biology and evolution of bacterial toxin-antitoxin systems. *Nat. Rev. Microbiol* **20**, 335–350 (2022).
3. Yarmolinsky, M. B. Programmed cell death in bacterial populations. *Science* **267**, 836–837 (1995).
4. Yamaguchi, Y. & Inouye, M. Regulation of growth and death in Escherichia coli by toxin-antitoxin systems. *Nat. Rev. Microbiol* **9**, 779–790 (2011).
5. Page, R. & Peti, W. Toxin-antitoxin systems in bacterial growth arrest and persistence. *Nat. Chem. Biol.* **12**, 208–214 (2016).
6. Harms, A., Brodersen, D. E., Mitarai, N. & Gerdes, K. Toxins, Targets, and Triggers: An Overview of Toxin-Antitoxin Biology. *Mol. Cell* **70**, 768–784 (2018).
7. LeRoux, M. & Laub, M. T. Toxin-Antitoxin Systems as Phage Defense Elements. *Annu Rev. Microbiol* **76**, 21–43 (2022).
8. Kelly, A., Arrowsmith, T. J., Went, S. C. & Blower, T. R. Toxin-antitoxin systems as mediators of phage defence and the implications for abortive infection. *Curr. Opin. Microbiol* **73**, 102293 (2023).
9. Guegler, C. K. & Laub, M. T. Shutoff of host transcription triggers a toxin-antitoxin system to cleave phage RNA and abort infection. *Mol. Cell* **81**, 2361–2373.e2369 (2021).
10. Zhang, T. et al. Direct activation of a bacterial innate immune system by a viral capsid protein. *Nature* **612**, 132–140 (2022).

11. LeRoux, M. et al. The DarTG toxin-antitoxin system provides phage defence by ADP-ribosylating viral DNA. *Nat. Microbiol* **7**, 1028–1040 (2022).

12. Bobonis, J. et al. Bacterial retrons encode phage-defending tripartite toxin-antitoxin systems. *Nature* **609**, 144–150 (2022).

13. Mets, T. et al. Mechanism of phage sensing and restriction by toxin-antitoxin-chaperone systems. *Cell Host Microbe* **32**, 1059–1073.e1058 (2024).

14. Kimelman, A. et al. A vast collection of microbial genes that are toxic to bacteria. *Genome Ress* **22**, 802–809 (2012).

15. Millman, A. et al. An expanded arsenal of immune systems that protect bacteria from phages. *Cell Host Microbe* **30**, 1556–1569.e1555 (2022).

16. Rousset, F. et al. Phages and their satellites encode hotspots of antiviral systems. *Cell Host Microbe* **30**, 740–753.e745 (2022).

17. Huang, H. et al. Divergence of structure and function in the haloacid dehalogenase enzyme superfamily: Bacteroides thetaiotaomicron BT2127 is an inorganic pyrophosphatase. *Biochemistry* **50**, 8937–8949 (2011).

18. Ozeir, M. et al. Structural basis for substrate selectivity and nucleophilic substitution mechanisms in human adenine phosphoribosyltransferase catalyzed reaction. *J. Biol. Chem.* **294**, 11980–11991 (2019).

19. Sinha, S. C. & Smith, J. L. The PRT protein family. *Curr. Opin. Struct. Biol.* **11**, 733–739 (2001).

20. Huyet, J. et al. Structural Insights into the Forward and Reverse Enzymatic Reactions in Human Adenine Phosphoribosyltransferase. *Cell Chem. Biol.* **25**, 666–676.e664 (2018).

21. Sharma, D. K., Misra, H. S., Bihani, S. C. & Rajpurohit, Y. S. Biochemical Properties and Roles of DprA Protein in Bacterial Natural Transformation, Virulence, and Pilin Variation. *J. Bacteriol.* **205**, e0046522 (2023).

22. Ahmad, S. I., Kirk, S. H. & Eisenstark, A. Thymine metabolism and thymineless death in prokaryotes and eukaryotes. *Annu Rev. Microbiol* **52**, 591–625 (1998).

23. Itsko, M. & Schaaper, R. M. dGTP starvation in Escherichia coli provides new insights into the thymineless-death phenomenon. *PLoS Genet* **10**, e1004310 (2014).

24. Briggs, G. S. et al. Ring structure of the Escherichia coli DNA-binding protein RdgC associated with recombination and replication fork repair. *J. Biol. Chem.* **282**, 12353–12357 (2007).

25. Wakamatsu, T. et al. Structure of RecJ exonuclease defines its specificity for single-stranded DNA. *J. Biol. Chem.* **285**, 9762–9769 (2010).

26. Romero, H. et al. Single molecule tracking reveals functions for RarA at replication forks but also independently from replication during DNA repair in Bacillus subtilis. *Sci. Rep.* **9**, 1997 (2019).

27. Keller, A. N. et al. Activation of Xer-recombination at dif: structural basis of the FtsKgamma-XerD interaction. *Sci. Rep.* **6**, 33357 (2016).

28. Uranga, L. A., Reyes, E. D., Patidar, P. L., Redman, L. N. & Lusetti, S. L. The cohesin-like RecN protein stimulates RecA-mediated recombinational repair of DNA double-strand breaks. *Nat. Commun.* **8**, 15282 (2017).

29. Stokar-Avihail, A. et al. Discovery of phage determinants that confer sensitivity to bacterial immune systems. *Cell* **186**, 1863–1876 e1816 (2023).

30. Hesselbach, B. A. & Nakada, D. Host shutoff" function of bacteriophage T7: involvement of T7 gene 2 and gene 0.7 in the inactivation of Escherichia coli RNA polymerase. *J. Virol.* **24**, 736–745 (1977).

31. Severinova, E. & Severinov, K. Localization of the Escherichia coli RNA polymerase beta' subunit residue phosphorylated by bacteriophage T7 kinase Gp0.7. *J. Bacteriol.* **188**, 3470–3476 (2006).

32. Tal, N. et al. Bacteria deplete deoxynucleotides to defend against bacteriophage infection. *Nat. Microbiol* **7**, 1200–1209 (2022).

33. Russell, C. W. & Mulvey, M. A. The Extraintestinal Pathogenic Escherichia coli Factor RqlI Constrains the Genotoxic Effects of the RecQ-Like Helicase RqlH. *PLoS Pathog.* **11**, e1005317 (2015).

34. Jiang, Y., Pogliano, J., Helinski, D. R. & Konieczny, I. ParE toxin encoded by the broad-host-range plasmid RK2 is an inhibitor of Escherichia coli gyrase. *Mol. Microbiol* **44**, 971–979 (2002).

35. Hsueh, B. Y. et al. Phage defence by deaminase-mediated depletion of deoxynucleotides in bacteria. *Nat. Microbiol* **7**, 1210–1220 (2022).

36. Hsueh, B. Y., Ferrell, M. J., Sanath-Kumar, R., Bedore, A. M. & Waters, C. M. Replication cycle timing determines phage sensitivity to a cytidine deaminase toxin/antitoxin bacterial defense system. *PLoS Pathog.* **19**, e1011195 (2023).

37. Bernard, P. & Couturier, M. Cell killing by the F plasmid CcdB protein involves poisoning of DNA-topoisomerase II complexes. *J. Mol. Biol.* **226**, 735–745 (1992).

38. Liu, Y., Wu, P., Li, B., Wang, W. & Zhu, B. Phosphoribosyltransferases and Their Roles in Plant Development and Abiotic Stress Response. *Int J Mol Sci* **24**, https://doi.org/10.3390/ijms241411828 (2023).

39. Minor, W., Cymborowski, M., Otwinowski, Z. & Chruszcz, M. HKL-3000: the integration of data reduction and structure solution-from diffraction images to an initial model in minutes. *Acta Crystallogr D. Biol. Crystallogr* **62**, 859–866 (2006).

40. Adams, P. D. et al. PHENIX: a comprehensive Python-based system for macromolecular structure solution. *Acta Crystallogr D. Biol. Crystallogr* **66**, 213–221 (2010).

41. Emsley, P. & Cowtan, K. Coot: model-building tools for molecular graphics. *Acta Crystallogr D. Biol. Crystallogr* **60**, 2126–2132 (2004).

42. Chen, V. B. et al. MolProbity: all-atom structure validation for macromolecular crystallography. *Acta Crystallogr D. Biol. Crystallogr* **66**, 12–21 (2010).

43. Li, H. & Durbin, R. Fast and accurate short read alignment with Burrows-Wheeler transform. *Bioinformatics* **25**, 1754–1760 (2009).

44. Abyzov, A., Urban, A. E., Snyder, M. & Gerstein, M. CNVnator: an approach to discover, genotype, and characterize typical and atypical CNVs from family and population genome sequencing. *Genome Res.* **21**, 974–984 (2011).

45. Cox, J. et al. Accurate proteome-wide label-free quantification by delayed normalization and maximal peptide ratio extraction, termed MaxLFQ. *Mol. Cell Proteom.* **13**, 2513–2526 (2014).

46. Tyanova, S., Temu, T. & Cox, J. The MaxQuant computational platform for mass spectrometry-based shotgun proteomics. *Nat. Protoc.* **11**, 2301–2319 (2016).

Acknowledgements

Author contributions

Q.C. and Y.Y. conceived and designed the experiments. H.P. and Y.C. performed experiments. X.Z. and L.D. performed mass spectrometry analysis. A.T. prepared the antibodies. H.P., D.T. Y.Y. and Q.C. analyzed the data. Q.C. and H.P. wrote the manuscript.

Competing interests

The authors declare no competing interests.

Additional information